PCCP

PAPER

View Article Online
View Journal | View Issue

Cite this: *Phys. Chem. Chem. Phys.*, 2022, **24**, 6453

Effect of the cation structure on the properties of homobaric imidazolium ionic liquids†

Spyridon Koutsoukos, [a] Frederik Philippi, [a] Daniel Rauber, [b] David Pugh, [c] Christopher W. M. Kay [bd] and Tom Welton *[a]

Received 11th November 2021,
Accepted 28th February 2022

DOI: 10.1039/d1cp05169e

rsc.li/pccp

In this work we investigate the structure–property relationships in a series of alkylimidazolium ionic liquids with almost identical molecular weight. Using a combination of theoretical calculations and experimental measurements, we have shown that re-arranging the alkyl side chain or adding functional groups results in quite distinct features in the resultant ILs. The synthesised ILs, although structurally very similar, cover a wide spectrum of properties ranging from highly fluid, glass forming liquids to high melting point crystalline salts. Theoretical *ab initio* calculations provide insight on minimum energy orientations for the cations, which then are compared to experimental X-ray crystallography measurements to extract information on hydrogen bonding and to verify our understanding of the studied structures. Molecular dynamics simulations of the simplest (core) ionic liquids are used in order to help us interpret our experimental results and understand better why methylation of C^2 position of the imidazolium ring results in ILs with such different properties compared to their non-methylated analogues.

Introduction

Modern chemistry is significantly focused on increasing sustainability *via* reduction in the cost and environmental footprint of chemical products and processes. Ionic liquids (ILs) have emerged as promising tools to achieve this goal, with much focus on synthetic, compound extraction or electrochemical processes.[1–5] The concept of 'designer solvents' has been developed in order to describe the synthetic flexibility of ILs and the aim of creating solvents with tailored properties to be a perfect match for specific applications.[6]

ILs, like other sustainability-related research fields, became a hotspot of academic interest when the need to improve existing industrial processes could no longer be neglected. This need has created a list of desirable properties for commercial applications, the search for which guides research.[7] Hundreds of researchers around the world are constantly looking for ILs with low viscosity, large electrochemical windows, long-term physical and chemical stability and low cost, aiming to replace currently used hazardous chemicals, while improving, or at least without any reduction in, process efficiency.[8–12]

This effort has led to the publication of many works studying the physical properties of series of IL structures and elucidating the structure–property relationships of these remarkable systems.[13,14] There are also literature reports on empirical models that try to predict ILs' properties, based either on group-contribution theory or on more complicated statistical computational correlations.[15–17] However, all of those models have some inherent restrictions in accuracy and/or precision of prediction, which result from the lack of complete understanding of how interactions between ions or specific functional groups affect the bulk properties of ILs.

Taking a closer look at such models, we can understand that their limitations arise from their being trained to fit existing experimental measurements, which in the case of ILs are somewhat desultory and often inconsistent. The result is that there are not enough useable data to extract accurate conclusions on structure–property relationships of ILs.[18] The available data are more sparse as the molecular weight of ILs increase (usually by increasing the size of the cation's alkyl side chain), as millions of structural isomers start to become possible, but they are even

[a] *Department of Chemistry, Molecular Sciences Research Hub, Imperial College London, White City Campus, London W12 0BZ, UK. E-mail: t.welton@imperial.ac.uk*
[b] *Department of Chemistry, Saarland University, Campus B2.2, 66123, Saarbrücken, Germany*
[c] *Department of Chemistry, Britannia House, Kings College London, 7 Trinity Street, London SE1 1DB, UK*
[d] *London Centre for Nanotechnology, University College London, 17-19 Gordon Street, London WC1H 0AH, UK*

† Electronic supplementary information (ESI) available: Synthetic procedures, ^{1}H and ^{13}C NMR spectra of synthesised ILs, raw data of physical measurements, TGA and DSC thermographs, *ab initio* calculations of non-synthesised cations, crystal structures of studied salts, source code, path beads, reference molecules, as well as further information about the methodology of MD simulations. CCDC 2120102–2120110. For ESI and crystallographic data in CIF or other electronic format see DOI: 10.1039/d1cp05169e

insufficient for smaller ions, for which the isomer count is more manageable. Another problem of studying properties of IL series of increasing molecular weight is that the functional group occupies a smaller percentage of the total mass, thus its effect on the overall electronic structure and intermolecular interactions will be quite different. Therefore, it makes sense to present a study of a series of ILs keeping the molecular weight unchanged as much as possible.[19]

It is also important to understand that the effect of a functional group is fundamentally dependent on its position in the ion. The work by Bonhote *et al.* shows relevant examples, where methylations of different parts of the imidazolium ring, or changing the relative positions of nitrogen cores in diazolium and triazolium cations cause significant changes to the physical properties of the resulting ILs.[20] This implies that one example of targeted structural modification of ions is not enough to characterise the whole chemical space and that it is definitely wrong to extrapolate the conclusions obtained from one family of structural isomers to another.

The molecular ions of which ionic liquids are composed, can usually exist in more than one conformation. Thus, the ions can change their overall shape, which facilitates structural relaxation. Two qualities – static and dynamic in origin – need to be discussed in this respect. First, which is the preferred minimum energy conformer of any given ion, what is its shape and relative energy? Second, what are the barriers separating the accessible conformers, *i.e.*, how fast can conformers interconvert?

The more conformers that are energetically accessible, the more entropy is introduced, which is beneficial for lowering liquefaction temperatures.[21,22] That being said, even in the liquid state the equivalent of a 'packing effect' can arise. A good example of this are the somewhat unexpected odd–even effects with increasing length of alkyl side chains.[23–25] However, if the energetic barriers that separate these conformers are too high, then the liquid essentially behaves like a mixture of differently shaped but rigid molecules. It is thus important to consider these energetic barriers as well.

Bearing these observations in mind, we performed a fundamental study of imidazolium ILs, to identify the effect of various structural modifications on their observed properties. As the starting point of our study we chose the widely-studied 1-propyl-3-methylimidazolium ($[C_3C_1im]^+$) cation, as this combines a low molecular weight and a small alkyl chain, which limits the number of structural isomers and conformational space, thus making a thorough explorative study more viable. All the studied cations have a less than 5% difference in their molecular weight compared to $[C_3C_1im]^+$, so practically this difference can be considered negligible. The chosen anions are halides (in principle the bromide anion, in some cases also chlorides for more thorough comparison) and the bis(trifluoromethylsulfonyl)imide ($[NTf_2]^-$) anion. Having such different anions (in terms of size, acidity, hydrogen bonding activity, *etc.*) will offer us a clearer image of how functionalisations and ion combinations affect the ILs' properties and whether these are affected by the overall environment and intermolecular interactions. We aim to see if the observed trends (*e.g.* melting point or viscosity change) are consistent between different ions and if they could be explained based on the interactions occurring between ions.

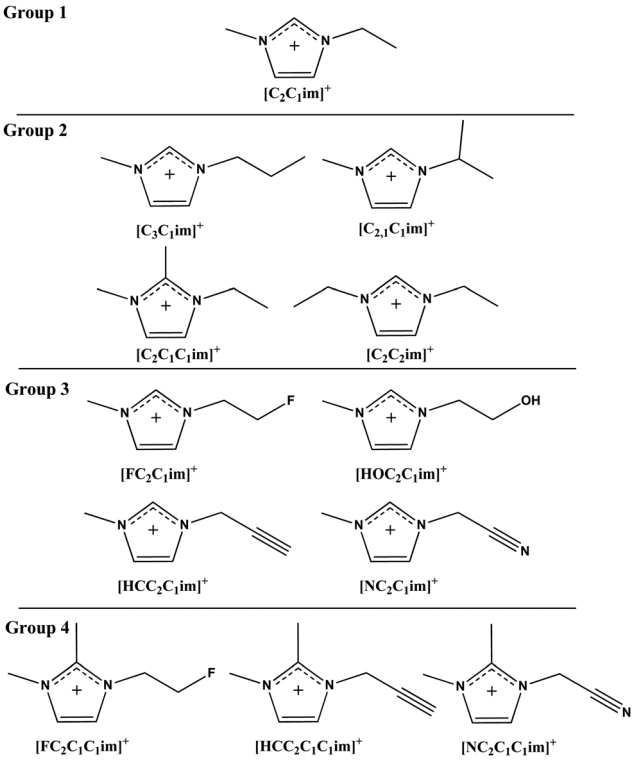

Fig. 1 Cation structures studied in this work and their abbreviations.

Fig. 1 shows the methodology used for the selection of structures studied in this work. First, we report the properties of $[C_2C_1im]^+$, which acts as a reference point (group 1), as it is one of the simplest and most widely studied IL cations. The second group of structures includes our model cation $[C_3C_1im]^+$, which was selected for the reasons explained above, as well as cation structures which are direct structural isomers of the model cation (group 2). The next group of cations includes functionalised cations with molecular weight comparable (less than 5% mass deviation) to that of $[C_3C_1im]^+$ (group 3). Similarly, the members of the last group also have comparable molecular weights, but also have a methylated C^2 position of the imidazolium ring (group 4). The methylated cations, evidently have a molecular weight that slightly deviates compared to the group 2 and 3 cations, however it is important to include them for a thorough comparison, as we intend to explore whether the properties of the functionalised ILs are closer to their methylated analogues rather than to each other. Moreover, adding an extra methyl group to the structure, and taking into account the molecular weight of the counterion, the methylated analogues deviate only around 5% from the model compound's molecular weight.

Materials and methods

Detailed descriptions of the synthetic procedures used in this work are provided in the ESI.† All ILs were dried *in vacuo* for a

few days before their use and they were handled in a glovebox or under Schlenk conditions. Coulometric Karl–Fischer titration showed a water content of <100 ppm for all samples.

Physicochemical characterisations

Thermal transitions. Phase transition points were measured on a DSC 1 STARe (Mettler Toledo, Gießen, Germany) which was equipped with a liquid nitrogen cooling system. Samples were weighed and hermetically sealed in Al-crucibles inside a glove box. The samples that were obtained in liquid state were heated to 100 °C with 5 °C min^{-1} and then cooled with −1 °C min^{-1} to −120 °C, held at this temperature for 5 minutes and then heated with +1 °C min^{-1} to ambient temperature. Samples that were obtained as solids after drying were heated up to 190 °C with a heating rate of +1 °C min^{-1} followed by a dynamic segment at the maximum temperature for 5 minutes and cooling again to 25 °C with a cooling rate of −1 °C min^{-1}. First-order transitions are given as the maximum of the peak, while the glass transition temperatures are determined using the midpoint method.

Thermogravimetric analysis (TGA). TGA measurements were performed on a Pyris1 TGA by PerkinElmer, equipped with a microbalance. 2–5 mg of sample were loaded on a platinum pan. The samples were left to equilibrate for 20 min at 50 °C, in order to remove all residual moisture. Then the samples were heated to 600 °C with 5 °C min^{-1} rate. N_2 was used as the carrier gas with 20 mL min^{-1} flow. The reported temperatures are T_{on}: onset temperature, calculated as the temperature point with 10% weight loss, $T_{max.\,rate}$: temperature with maximum decomposition rate, obtained by the first derivative of the thermogram and $T_{1/2}$: temperature of 50% weight loss of the sample.

TGA/MS measurements were performed on a TGA/DSC 1 STARe (Mettler Toledo, Gießen, Germany) equipped with a quadrupole mass spectrometer QMA-125 from Balzers. The same method as described above was used for the TGA/MS measurement.

Dynamic viscosity. Dynamic viscosity was measured under flow of dry nitrogen to avoid uptake of moisture using a MCR 301 Rheometer (Anton Paar, Graz, Austria) with cone–plate geometry. The particular measuring system was a CP50-1 cone (49.95 mm diameter, cone angle 1°) with a gap size of 0.101 mm. The viscosity was measured in 5 °C steps from 25 °C to 105 °C. For each temperature 30 points were measured for shear rates ranging from 50 to 150 s^{-1} (linear ramp) with a duration of 15 s per measured shear rate. As there was no shear rate dependence in the investigated shear rate region, thus Newtonian flow behaviour, the values per temperature were averaged.

Density measurements. Densities were measured from 25 °C to 95 °C in 10 °C steps using a pycnometer and an Proline RP 1845 thermostat bath (LAUDA, Lauda-Königshofen, Germany) with T-stability of ±0.01 °C as reported in previous publications.[12,26]

Self-diffusion coefficients. Pulsed field gradient stimulated echo (PFGSTE) NMR spectra were recorded on a Bruker Avance III HD 500 equipped with 5 mm BBO SmartProbe at 297 K. All spectra were recorded on neat and degassed ILs with an external DMSO-d_6 capillary. The followed procedure is explained in detail in a previous publication from our group.[27]

X-ray crystallography. Datasets were collected using the following hardware: [N≡C_2C_1im]Cl: an Oxford Diffraction PX Ultra diffractometer (Cu Kα radiation, 1.54184 Å); [N≡C_2C_1im]Br, [HC≡$C_2C_1C_1$im]Br, [HC≡C_2C_1im]Br, [N≡$C_2C_1C_1$im]Br, [N≡$C_2C_1C_1$im][NTf_2], [N≡$C_2C_1C_1$im]Cl, and [HOC_2C_1im]Br: an Oxford Diffraction Xcalibur 3E (Mo Kα radiation, 0.71073 Å). Data processing was carried out using CrysAlisPro,[28] solutions were solved and refined using Olex-2.[29] Hydrogen atoms were placed in geometrically assigned positions with C–H distances of 0.95 Å (CH), 0.97 Å (CH_2) or 0.98 Å (CH_3) and refined using a riding model, with $U_{iso}(H) = 1.2U_{eq}(C)$ (CH, CH_2) or $1.5U_{eq}(C)$ (CH_3). Graphics were generated using Olex-2 and Mercury.[30] 2120102 ([N≡C_2C_1im]Br), 2120103 ([HC≡$C_2C_1C_1$im]Br), 2120104 ([HC≡C_2C_1im]Br), 2120105 ([N≡$C_2C_1C_1$im]Br), 2120106 ([N≡$C_2C_1C_1$im][NTf_2]), 2120107 ([N≡C_2C_1im]Cl), 2120108 ([N≡$C_2C_1C_1$im]Cl), 2120109 ([HOC_2C_1im]Br) and 2120110 ([$C_2C_1C_1$im]Br) contain crystallographic data in CIF format, which is also summarised below (also Table S8 – ESI†).

[N≡$C_2C_1C_1$im][NTf_2] and [HOC_2C_1im]Br were both refined as 2-component twins. One of the fluorine atoms in [N≡$C_2C_1C_1$im][NTf_2] also needed isotropic restraints to maintain a sensible geometry.

In order to prepare crystals suitable for X-ray crystallography, the dried compound was dissolved in the minimum amount of either acetone or butanol and the solvent was left to evaporate over the several days under nitrogen flow at room temperature.

***Ab initio* calculations.** *Ab initio* calculations were performed at the full MP2/cc-pVTZ//B3LYP-GD3BJ/6-311+g(d,p) level of theory using the Gaussian software package, Revision D.01.[31–33] The methodology is described in detail in a previous publication.[27] Briefly, to obtain the potential energy curves, geometry optimisations were carried out by relaxing all coordinates except the dihedral angle of interest. For each potential energy curve, 72 dihedral angles were chosen from 0° to 360° in steps of 5°. A full MP2 single point calculation was then performed for each of these structures to obtain the energy. Geometry optimisations used the default SCF convergence criterion of 10^{-8} on the (RMS) density matrix and 10^{-6} on the energy. For the MP2 calculations, a tightened convergence criterion of 10^{-10} on the (RMS) density matrix and 10^{-8} on the energy was used. No symmetry was applied for any of the calculations. Input *z*-matrices and the energies as a function of dihedral angles are given in the ESI.†

MD simulation

Classical all-atom molecular dynamics simulations were performed using the ttdamp branch of the LAMMPS software package (7Aug2019) with periodic boundary conditions.[34] Since the official release version 29Oct2019, the required features are part of the USER-DRUDE package of the main branch of LAMMPS.[35] A cutoff of 12 Å was used for (non-bonded) pair interactions, including tail corrections for energy and pressure.[36] Long range electrostatic interactions were computed with the particle–particle particle-mesh method with relative

force error of 10^{-6}. Non-bonded interactions between atoms separated by one, two, or three bonds were scaled with 0.0, 0.0, and 0.5, respectively. The SHAKE algorithm with a tolerance of 10^{-4} limited to 20 iterations was used to constrain C–H bonds to their equilibrium value.[37] Simulations were performed in the *NPT* or *NVT* ensembles using a timestep of 0.5 fs. A skin distance of 2 Å was used to rebuild neighbour lists. Linear momentum of the centre of mass movement of the whole simulation box was removed every 1000 steps without velocity rescaling.

The (non-polarisable) CL&P force field is used as a basis for the (polarisable) CL&Pol force field employed in this work.[38–40] The CL&Pol force field uses Drude particles in the extended Lagrangian approach with a temperature grouped dual Nosé–Hoover chain thermostat as described by Goloviznina *et al.*, including the Martyna–Tuckerman–Klein correction.[35,41–45] Here, the (internal) degrees of freedom of the Drude particles relative to their respective cores were thermostatted at 1 K, whereas all other (real) degrees of freedom were thermostatted at 298.15 K. The chain length of the thermostat was 3, and the temperature damping parameters were 100 fs for real degrees of freedom and 25 fs for internal Drude degrees of freedom. The pressure damping parameter for *NPT* simulations was 1000 fs. The mass of Drude particles was set to 0.4 g mol^{-1}, which was subtracted from the respective core. The core-Drude force constant was set to 1000 kcal mol^{-1} $Å^{-2}$.[46] The charges on Drude particles were calculated from atomic polarisabilities as $q = \sqrt{\alpha \cdot k_{DP}}$.[46,47] The sum of Drude and core charges gives the charge of the corresponding atomic site in the CL&P force field. To avoid double counting of inductive effects, the Lennard-Jones ε parameters were scaled by 0.65 for both $[C_2C_1im][NTf_2]$ and $[C_2C_1C_1im][NTf_2]$ as described in the literature.[48,49] The $[C_2C_1C_1im][NTf_2]$ scaling factor obtained from the predictive scheme following the literature protocol, including the optimisation of the dimer at the B97-D3/cc-pVDZ level of theory, was found to be 0.57.[48] However, we observed that this scaling factor produced unrealistically fast dynamics, with diffusion coefficients exceeding those of the simulation of $[C_2C_1im][NTf_2]$. Hence, we decided to use the same scaling factor for both simulations, which produces simulated diffusion coefficients that follow the experimentally observed trends (see ESI†). The key results obtained from the MD simulation remain the same for both scaling factors (see ESI†). Our source code, path beads, reference molecules, as well as further information about the methodology are provided in the ESI.†

Results and discussions

Thermal behaviour

Investigating the thermal transitions of ILs is of utmost importance for their applications, as the high melting points of some salts are the bottleneck that prevents their use in most applications. The observed melting points (T_m), crystallisation points (T_c), as well as the glass transition temperatures (T_g) are reported in Table 1. The studied ILs include two main categories, the halide salts (here with Br^- and Cl^- anions) that generally have high melting points and the bis(trifluoromethylsulfonyl)imide ILs that have low melting points (usually they are liquid close to room temperature, with the exceptions of $[FC_2C_1C_1im][NTf_2]$, $[HC{\equiv}C_2C_1C_1im][NTf_2]$ and $[N{\equiv}C_2C_1C_1im][NTf_2]$). Our reference ILs, which have the simplest structure among the studied series, are the those with the $[C_3C_1im]^+$ cation and show only T_g with both Br^- and $[NTf_2]^-$ anions. The C^2-methylated isomers $[C_2C_1C_1im]Br$ and $[C_2C_1C_1im][NTf_2]$, both exhibit crystallisation (at various temperatures depending on each case). For the analogues which have been functionalised in the alkyl chain, we observe that F- and HO-functionalisations result in glass forming ILs, while the triple bond functionalisations result in ILs that crystallise. An exception to this observation is $[N{\equiv}C_2C_1im][NTf_2]$, which is a glass-forming IL, although the halides (both Br^- and Cl^-) are crystal-forming salts. Another very interesting observation is the case of $[N{\equiv}C_2C_1C_1im][NTf_2]$, which shows an unexpectedly high melting point, which however is not the case for $[HC{\equiv}C_2C_1C_1im][NTf_2]$. The origins of this behaviour are investigated and further discussed below.

Table 1 DSC data for the studied ILs

IL	T_c (°C)	T_m (°C)	ΔH_f[b] (kJ mol^{-1})	ΔS_f[c] (J mol^{-1} K^{-1})	T_g (°C)
$[C_2C_1im]Br$	24	67	14.06	41.33	—
$[C_2C_1C_1im]Br$	53	102	9.60	25.60	—
$[C_3C_1im]Br$	—	—	—	—	−54
$[C_2C_2im]Br$	21	68	9.14	26.8	—
$[HOC_2C_1im]Br$	3	90	12.77	35.16	—
$[C_{2,1}C_1im]Br$	10[a]	77	13.94	39.80	−43
$[C_{2,1}C_1C_1im]Br$	182	187	21.75	47.26	—
$[FC_2C_1im]Br$	—	—	—	—	−44
$[FC_2C_1C_1im]Br$	—	114	14.39	37.17	—
$[HC{\equiv}C_2C_1im]Br$	—	72	13.11	37.98	—
$[HC{\equiv}C_2C_1C_1im]Br$	71	180	19.66	43.38	—
$[N{\equiv}C_2C_1im]Br$	130	167	24.89	56.54	—
$[N{\equiv}C_2C_1im]Cl$	75	170	22.51	50.79	—
$[N{\equiv}C_2C_1C_1im]Br$	143	177	22.58	50.15	—
$[N{\equiv}C_2C_1C_1im]Cl$	81	145	22.27	53.26	—
$[C_2C_1im][NTf_2]$	−38	−15	21.56	83.51	—
$[C_2C_1C_1im][NTf_2]$	−8	25	13.57	45.51	—
$[C_3C_1im][NTf_2]$	—	—	—	—	−92
$[C_2C_2im][NTf_2]$	−27	17	30.78	106.1	—
$[HOC_2C_1im][NTf_2]$	—	—	—	—	−79
$[C_{2,1}C_1im][NTf_2]$	−21	13	19.10	66.74	—
$[C_{2,1}C_1C_1im][NTf_2]$	−43	29	15.51	51.33	—
$[FC_2C_1im][NTf_2]$	—	—	—	—	−81
$[FC_2C_1C_1im][NTf_2]$	−33	32	18.47	60.52	—
$[HC{\equiv}C_2C_1im][NTf_2]$	−15	13	19.26	67.31	—
$[HC{\equiv}C_2C_1C_1im][NTf_2]$	−30	39	21.75	69.68	—
$[N{\equiv}C_2C_1im][NTf_2]$	—	—	—	—	−57
$[N{\equiv}C_2C_1C_1im][NTf_2]$	12	70	17.28	50.34	—

[a] Cold crystallisation. [b] Enthalpy is calculated as the area under the curve for the melting transition as kJ mol^{-1}. [c] Entropy is calculated from the enthalpy divided by T_m.

TGA analysis

TGAs reveal that the decomposition profiles significantly change among the studied samples. As expected by other analogous studies,[50] ILs with methylated ring positions decompose at slightly higher temperatures compared to their corresponding non-methylated analogues (Table 2). The

Table 2 Summary table of T_{on}, $T_{1/2}$, $T_{max.rate}$ and carbon residue of studied ILs

IL	T_{on} (°C)	$T_{1/2}$ (°C)	$T_{max.rate}$ (°C)	Carb. residue (% weight)
$[C_2C_1im]Br$	262.5	294.5	304.1	0
$[C_2C_1C_1im]Br$	275.4	305.8	312.8	0.8
$[C_3C_1im]Br$	267.3	296.9	304.9	0
$[HOC_2C_1im]Br$	293.2	315.1	315.0	7.8
$[C_{2,1}C_1im]Br$	275.0	302.0	309.9	0
$[C_2C_2im]Br$	267.6	296.2	304.3	0.8
$[C_{2,1}C_1C_1im]Br$	281.1	309.9	316.5	0.6
$[FC_2C_1im]Br$	236.0	297.6	302.8	9.1
$[FC_2C_1C_1im]Br$	250.4	318.2	320.6	13.2
$[HC\equiv C_2C_1im]Br$	253.7	296.8	294.0	25.4
$[HC\equiv C_2C_1C_1im]Br$	279.6	323.2	323.5	22.3
$[N\equiv C_2C_1im]Br$	251.3	286.6	296.6	23.6
$[N\equiv C_2C_1im]Cl$	233.1	268.5	270.9	30.9
$[N\equiv C_2C_1C_1im]Br$	264.9	300.9	307.6	19.5
$[N\equiv C_2C_1C_1im]Cl$	253.2	305.6	314.9	30
$[C_2C_1im][NTf_2]$	381.5	434.5	453.5	1.2
$[C_2C_1C_1im][NTf_2]$	382.3	420.9	434.0	1.8
$[C_3C_1im][NTf_2]$	384.2	440.3	455.8	1.8
$[HOC_2C_1im][NTf_2]$	411.1	445.2	461.7	8.0
$[C_{2,1}C_1im][NTf_2]$	348.6	394.3	406.3	0.6
$[C_2C_2im][NTf_2]$	381.9	434.8	453.1	1.2
$[C_{2,1}C_1C_1im][NTf_2]$	373.8	421.3	436.0	1.1
$[FC_2C_1im][NTf_2]$	370.9	429.8	445.5	3.5
$[FC_2C_1C_1im][NTf_2]$	401.8	446.9	455.1	6.8
$[HC\equiv C_2C_1im][NTf_2]$	353.6	402.1	408.0	14.1
$[HC\equiv C_2C_1C_1im][NTf_2]$	378.4	428.1	431.3	13.9
$[N\equiv C_2C_1im][NTf_2]$	373.3	412.2	416.7	9.9
$[N\equiv C_2C_1C_1im][NTf_2]$	385.9	418.4	426.9	9.9

HO-functionalised ILs decompose at significantly higher temperature compared to the other ILs, while the F-functionalised salts do not deviate significantly compared to the non-functionalised chains. Furthermore, the triple bond functionalised ILs (both alkyne and nitrile chains) leave higher carbon residue compared to the non-functionalised, for which it is almost zero. This effect is more apparent for the halides (residue in the range of 20–30%) compared to the bis(trifluoromethylsulfonyl)imide ILs (residue in the range of 10–15%). This is an indication that the decomposition pathway for those is different, probably heavier decomposition products are produced as a result of chain polymerisation.[51]

According to Lovelock *et al.*,[52] during thermal decomposition of methylimidazolium halides a nucleophilic attack of the halide anion is favourable and the decomposition products are mostly composed of the alkyl halide fragments (from both alkyl chains) and the resulting alkylimidazoles. This pathway seems to make sense for the results of the ILs with non-functionalised cations, as well as for the HO-functionalised chains. However, this is not the case for the triple bond functionalised chains. It is possible that at such high temperatures, polymerisation of the side chain occurs and instead of the formation of volatile alkyl halides, the polymerisation products stay in the bulk and decompose further – which results in higher carbonaceous residue.[53] According to the literature, cyclisation is the main reaction occurring for polyacrylonitriles in the temperature range of 180 to 240 °C.[54] The final products from this reaction are various imine structures through oligomerisation of the nitrile groups. In order to investigate if this is indeed the case in our system we heated the ILs to 200 °C for a few hours which resulted in a dark-coloured sticky product without any significant mass loss, which is an indication that such polymerisation reactions are taking place.

According to the same study by Lovelock *et al.*, for the $[NTf_2]^-$ salts only evaporation of the ILs as neutral ion pairs was observed.[52] Again, this does not seem to be the case for the alkyne and nitrile functionalised ILs. Their carbon residue is around 10–15%, which is in the same weight range as observed for the halide salts if we consider the percentage contribution of the side chain mass to the IL's molar mass. This supports the suggestion that these side chains remain as polymerised materials and also shows that this reaction is probably due to the high temperature conditions and is not affected significantly by the basicity of the anion. High carbonaceous residue upon pyrolysis of similar ILs has also been observed by Lee *et al.*,[55] who successfully used them as precursors for the formation of carbon nanomaterials.[56]

$[FC_2C_1im]^+$ and $[FC_2C_1C_1im]^+$ cations are another special case which seem to have a different decomposition pathway. As we can see from Fig. S30–S33 (ESI†), the bromide salts decompose in two steps, which however is not the case for the $[NTf_2]^-$ ILs. TGA/MS of the halide salts (Fig. S34 – see ESI†) reveals a total decomposition of the cation during the thermal heating, which explains the two distinct decomposition steps. For $[FC_2C_1im]Br$ we observe an initial production of CH_3Br (m/z ES^+ 93, 95), which corresponds to the first decomposition step, with the simultaneous production of imidazole (m/z ES^+ 67, 68). $[FC_2C_1C_1im]Br$ follows the same decomposition pathway, as we observe the release of CH_3Br, as well as the corresponding 2-methylimidazole (m/z ES^+ 81). We did not observe any traces of the fluorinated side chain, but it could react and form further by-products which are outside of the instrument's detection limits. The complete decomposition of the IL structure significantly deviates from the decomposition mechanisms mentioned above.

Densities

The densities of the 2-methylated analogues are consistently lower than the corresponding non-methylated ILs. For the methylated analogues density increases as follows (Fig. 2): $[C_{2,1}C_1C_1im]^+ < [C_2C_1C_1im]^+ < [FC_2C_1C_1im]^+$. We have to note here that the densities and viscosities of $[HC\equiv C_2C_1C_1im][NTf_2]$ and $[N\equiv C_2C_1C_1im][NTf_2]$ salts were not measured, as these are solid at room temperature.

The densities of the non-methylated analogues have the following trend: $[C_3C_1im]^+ = [C_{2,1}C_1im]^+ = [C_2C_2im]^+ < [C_2C_1im]^+ < [HC\equiv C_2C_1im]^+ < [HOC_2C_1im]^+ < [FC_2C_1im]^+ < [N\equiv C_2C_1im]^+$. It is important to note that the density fitted lines are parallel for the studied range, so the trend is the same for both low and high temperatures. Here we observe that ILs with n-propyl and isopropyl side chains, as well as the symmetric $[C_2C_2im]^+$ have almost identical densities, effectively showing that the re-arrangement of carbons in the side chains does not affect the amount of space they occupy. This indicates that the arrangement of the side chain carbons doesn't affect the density of the IL. On the other hand, adding a functional group on the side chain does alter the properties. The hydroxyl-functionalised IL shows considerably

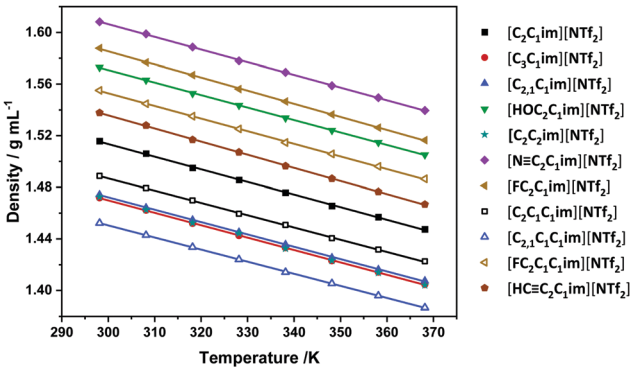

Fig. 2 Densities of studied bis(trifluoromethylsulfonyl)imide ILs.

higher density, followed by the fluorinated IL. The triple bond functionalised ILs again have higher densities compared to the non-functionalised analogues, with the nitrile group showing the highest density among all studied ILs. However, since as discussed in the introduction section, not all the ILs have identical weight, we considered it safer to use molar volumes rather than densities for comparison (see below), since normalisation to molar volumes will eliminate the fluctuations that are due to the differences in molar mass of the cation.

Molar volumes

The transformation of densities to molar volumes results in some ILs being grouped together (Fig. 3), providing us with clearer insight of the various functionalisation effects on the systems. Molar volumes of 2-methylated ILs are consistently higher than their non-methylated analogues. As expected, since the densities are the same, the molar volumes of n-propyl and isopropyl ILs are also identical. This result was also observed in the work of Zhang *et al.*[57] and Xue *et al.*,[58] where ILs with same number of carbons showed identical density, regardless of the existence of linear or branched side chain. An interesting observation is that the molar volumes for $[HOC_2C_1im]^+$, $[FC_2C_1im]^+$ and $[C_2C_1im]^+$ overlap, which indicates that the functionalisation of the alkyl side chain doesn't affect this property, as the volume occupied by the molecules remains unchanged. Similar observation remains for the 2-methylated analogues of those cations, as the molar volumes of

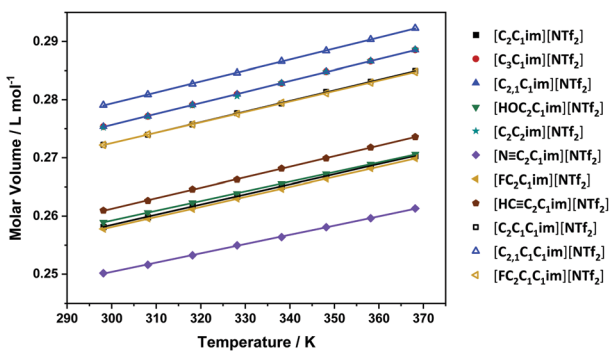

Fig. 3 Molar volumes of studied bis(trifluoromethylsulfonyl)imide ILs.

$[FC_2C_1C_1im]^+$ and $[C_2C_1C_1im]^+$ also overlap. Comparing the group of structural isomer cations (Fig. 1 – group 2) we observe that methylation of C^2 position results in slightly reduced molar volume of $[C_2C_1C_1im]^+$ compared to the other two isomers (0.270 compared to 0.275 L mol^{-1} at 298 K). Study of molar volumes also reveals that $[HOC_2C_1im]^+$ is closer to $[C_2C_1im]^+$ than $[C_3C_1im]^+$. This observation makes sense if we think in terms of packing efficiency. Increasing the length of the side chain by one carbon, we increase the non-polar part of the molecule, which is known to promote the formation of heterogeneous environments,[59] thus the IL packs less efficiently and the molecules occupy more space (higher molar volume). However, replacing a carbon with a hydroxyl group seems to negate that effect, probably because the hydroxyl group's polar nature and hydrogen bonding ability further helps in the packing of ions, whilst simultaneously reducing the likelihood of any nanosegregation. This position is further supported when also comparing the case of $[FC_2C_1im]^+$, which is closer to $[C_3C_1im]^+$. Possibly the absence of hydrogen bonding terminal group makes fluorine to practically have similar effect in terms of packing as adding an extra carbon.

It is also very interesting to compare the changes in triple-bond functionalisation of the ILs compared to $[C_3C_1im]^+$. Both ILs have reduced molar volume compared to the model cation, however alkyne functionalisation has smaller effect (0.260 L mol^{-1} at 298 K) than the nitrile group (0.250 L mol^{-1} at 298 K). This is a very good indication that the existence of the triple bond itself does not determine the properties of the IL, but the nature of the atoms significantly changes the interactions. This will be further discussed below, along with the theoretical calculations on these systems.

Viscosities

The temperature dependence of the studied viscosities can be efficiently described ($R^2 > 0.99999$ in all cases) by the Vogel–Fulcher–Tammann (VFT) equation for the whole studied range. The fitting parameters can be found in Tables S5–S7 in the ESI,† while the data together with the fitted curves are shown on Fig. 4. As expected, the lowest viscosity at 25 °C was found for $[C_2C_1im][NTf_2]$, which however also has a lower molecular weight compared to the other ILs. The 2-methylated ILs have consistently higher viscosities compared to their non-methylated analogues. Their trend, in terms of increasing viscosity, is $[C_2C_1C_1im]^+ < [C_{2,1}C_1C_1im]^+ < [FC_2C_1C_1im]^+$. The trend followed by the non-methylated ILs (and excluding $[C_2C_1im][NTf_2]$) is $[C_2C_2im]^+ < [C_3C_1im]^+ = [C_{2,1}C_1im]^+ < [HC{\equiv}C_2C_1im]^+ < [FC_2C_1im]^+ < [HOC_2C_1im]^+ < [N{\equiv}C_2C_1im]^+$. Similarly to densities, both non-functionalised propyl-substituted ILs have identical viscosities, which again shows that the n- or iso-arrangement of the alkyl side chain doesn't significantly affect the rheological properties of the liquid in this case. Comparing just the group of structural isomers, we observe that the methylated isomer ($[C_2C_1C_1im]^+$) appears more viscous than the others, while the symmetric $[C_2C_2im]^+$ is more fluid, practically identical to $[C_2C_1im]^+$. Taking into account the fact that the density remained

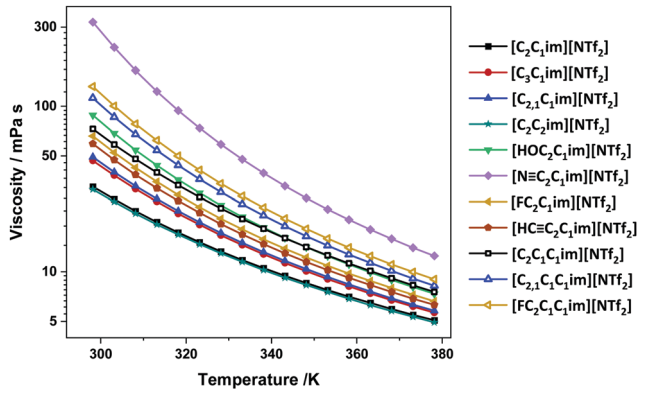

Fig. 4 Viscosities of studied bis(trifluoromethylsulfonyl)imide ILs.

unaffected by the carbon re-arrangement, it seems that the increased fluidity of $[C_2C_2im]^+$ is not due to increased free space; the cation benefits from the existence of flexible chains in both sides of the ring instead of just one. It is known that the conformational flexibility around the C–N bond connecting the imidazolium ring with the alkyl chain significantly increases the diffusion rates of alkylimidazolium cations, more than what the rotation around other bonds of the side chain does.[60] Moving forward to groups 3 and 4, we see that the fluorinated IL shows higher viscosity compared to the non-functionalised, followed by the HO-functionalised IL. $[HOC_2C_1im][NTf_2]$ is one of the two group 3 ILs which are more viscous than $[C_2C_1C_1im][NTf_2]$. This is a clear indication that the extra hydrogen bonds due to the hydroxyl group make the ILs less fluid. The other IL that belongs to this category is $[N{\equiv}C_2C_1im][NTf_2]$. Regarding the triple bond functionalised ILs, the alkyne group makes the ILs more viscous compared to the non-functionalised analogues, but significantly less viscous than the other functionalised analogues. The nitrile group creates the most viscous of all the studied ILs, an observation that will be further discussed below.

From the performed study we see two independent effects of intermolecular interactions on the bulk properties. Methylation of the C^2 position of the imidazolium ring, although it significantly reduces the hydrogen bonding ability of the IL (C^2–H is considered as the primary hydrogen bonding site of the imidazolium ring[61]), it creates more viscous and denser ILs.[62] Adding additional interaction sites increases viscosity (such as the case of $[HOC_2C_1im]^+$ with additional hydrogen bonding, or $[N{\equiv}C_2C_1im]^+$ which promotes additional dipole–dipole interactions), but effects on density and molecular volume vary significantly, due to the nature and the extent of the interaction.

Self-diffusion of ions

The self-diffusion coefficients present an especially interesting property, since we are able to investigate the behaviour of the cation and the anion independently. Previous research has shown that around room temperature, in short-chain imidazolium ILs, the cation tends to diffuse faster than the anion.[63,64] This observation is in agreement with our measurements (Table 3), as in all cases the anion diffuses consistently slower than the cation. The diffusion trend based on the cations is: $[C_2C_2im]^+ > [C_2C_1im]^+ > [C_3C_1im]^+ > [C_{2,1}C_1im]^+ > [HC{\equiv}C_2C_1im]^+ > [FC_2C_1im]^+ > [C_2C_1C_1im]^+ > [HOC_2C_1im]^+ > [C_{2,1}C_1C_1im]^+ > [FC_2C_1C_1im]^+ > [N{\equiv}C_2C_1im]^+$. The trend is identical for the anions in these ILs, while the diffusion coefficient values of the anions are lower by around 30% on average, compared to the cation diffusions.

Table 3 Anion and cation self-diffusion coefficients for the NTf_2 ILs that are liquid at room temperature

Ionic liquid	Cation self-diffusion D_+ (10^{-11} m^2 s^{-1})	Anion self-diffusion D_- (10^{-11} m^2 s^{-1})
$[C_2C_1im][NTf_2]$	5.1	2.8
$[C_2C_1C_1im][NTf_2]$	2.3	1.5
$[C_3C_1im][NTf_2]$	3.6	2.3
$[C_{2,1}C_1im][NTf_2]$	3.3	2.2
$[C_{2,1}C_1C_1im][NTf_2]$	1.4	0.92
$[C_2C_2im][NTf_2]$	5.8	3.4
$[HOC_2C_1im][NTf_2]$	1.8	1.2
$[FC_2C_1im][NTf_2]$	2.5	1.6
$[FC_2C_1C_1im][NTf_2]$	1.2	0.84
$[HC{\equiv}C_2C_1im][NTf_2]$	2.7	1.9
$[N{\equiv}C_2C_1im][NTf_2]$	0.46	0.37

Similar to the previously studied properties, methylation of 2-position of the imidazolium ring makes the ionic liquids' ions diffuse slower than their non-methylated analogues. An unexpected result here is that the symmetric $[C_2C_2im]^+$ diffuses even faster than the lighter $[C_2C_1im]^+$. Taking into account group 2 ILs, we observe that $[C_2C_1C_1im]^+$ diffuses significantly slower than the other isomers. Regarding group 3 and 4 ILs, we observe that all ILs diffuse slower than those with non-functionalised side chains. However, F- and alkyne functionalisations only slightly decrease the diffusion coefficients (2.5 and 2.7 $\times$ 10^{-11} m^2 s^{-1}, respectively) compared to $[C_3C_1im]^+$ (3.6 $\times$ 10^{-11} m^2 s^{-1}), while HO- and nitrile functionalisations cause more significant reductions (1.8 and 0.46 $\times$ 10^{-11} m^2 s^{-1}, respectively). This observation further supports our proposition that HO- and nitrile functionalisations increase the system's ordering, leading to slower dynamics.

Studies of conformational space

For the short-chain imidazolium ionic liquids in this work, the major changes in shape arise from rotation around the N–C bond where the side chain is attached to the imidazolium core. We will use the corresponding dihedral angle, starting from the C^2 carbon of the imidazolium core (carbon between the two nitrogens) and extending along the backbone of the side chain, as a measure for the conformation of the cation. Fig. 5 shows $[C_3C_1im]^+$ as an example, with C–N–C–C dihedral angles of 0° and 90°. For some cations such as $[C_2C_1im]^+$, this dihedral is sufficient to sample all minimum conformers. For longer flexible side chains, such as $[C_3C_1im]^+$, more conformers arise due to rotation around C–C bonds further along the chain. However, the rotation around the C–N bond – and the ease with which this rotation can take place – is a key factor influencing dynamic properties such as diffusion for imidazolium ionic liquids.[60,65]

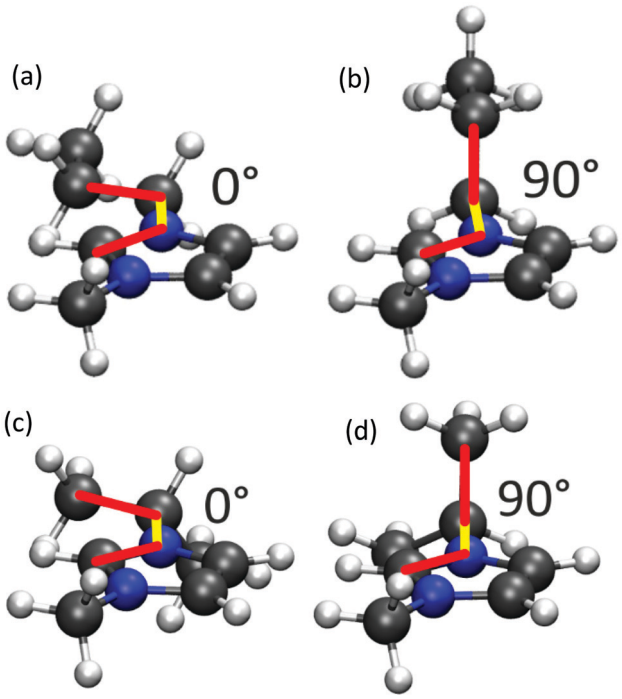

Fig. 5 Example of $[C_3C_1im]^+$ cation in 0° (a) and 90° (b) and $[C_{2,1}C_1im]^+$ cation in 0° (c) and 90° (d) C–N–C–C dihedral angle arrangements. The C–N bond is highlighted in yellow, the neighbouring bonds which we use to define the dihedrals in this work are highlighted in red. The dihedral angle is obtained as the angle between the vector projections of the vectors corresponding to the red bonds from the vector corresponding to the yellow bond. (The origins of the red vectors are the points shared with the yellow bond vector.)

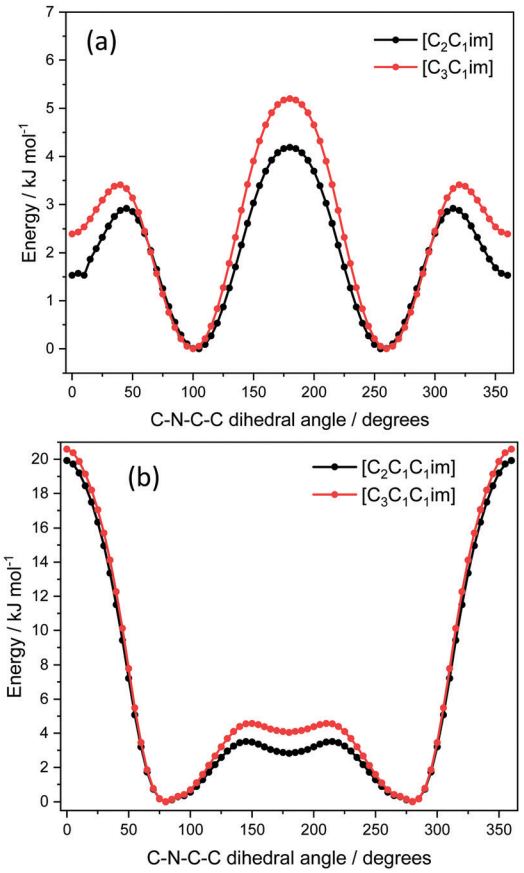

Fig. 6 *Ab initio* energy calculation of C–N–C–C dihedral angle for (a) $[C_2C_1im]^+$ (black), $[C_3C_1im]^+$ (red) and (b) $[C_2C_1C_1im]^+$ (black) and $[C_3C_1C_1im]^+$ (red) cations.

Fig. 6 shows the effect of an additional methyl group, extending the linear alkyl side chain. The local minima appear at the same angles, but the energy barriers slightly increase with the addition of the extra group. The changes in energy are small and comparable to the accuracy of the method, thus is can be expected that the additional degree of freedom in the propyl chain has a larger (beneficial) impact on the properties than the loss in flexibility for rotation around the C–N bond. Comparing Fig. 6(a) and (b), we observe the effect of methylation at the C^2 position of the imidazolium ring on the minimum geometries and the energy barriers. For the non-methylated analogues, an angle of 0° (360°) angle corresponds to a local minimum, which however is transformed to a global maximum upon methylation due to the steric clash. It is therefore apparent that the flat arrangement of the molecules is not favourable for C^2-methylated rings. The energy barrier for rotation of the side chain around the C^2-side is increased significantly to around 20 kJ mol^{-1}. Thus, only rotation around the $C^{4/5}$ side of the cation is feasible.

Fig. 7 shows the energy profiles comparison between $[C_3C_1im]^+$ and $[C_{2,1}C_1im]^+$, two cations that create a very interesting case for comparison, as they have identical molecular weight and their only difference is the existence of branched side chain instead of linear. Taking a closer look at the obtained experimental data for these cations, we see that for the halide analogues, $[C_3C_1im]Br$ is a viscous liquid with T_g of −54 °C, while $[C_{2,1}C_1im]Br$ is a solid with T_m of 77 °C and T_g of −43 °C. Similar differences still exist for the $[NTf_2]^-$ analogues, with $[C_3C_1im][NTf_2]$ being a liquid with T_g of −92 °C, while $[C_{2,1}C_1im][NTf_2]$ is a crystalline solid that melts above 13 °C. Interesting enough, the transport properties of these liquids are

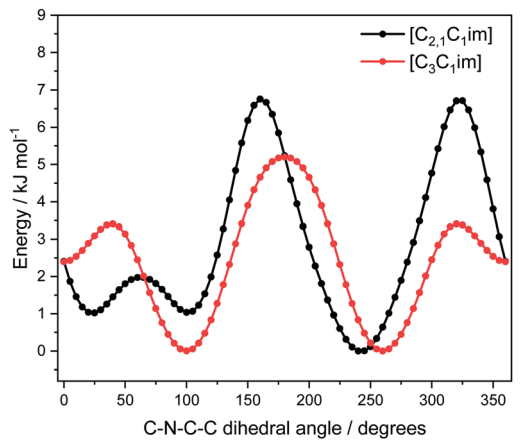

Fig. 7 *Ab initio* energy calculation of C–N–C–C dihedral angle for $[C_3C_1im]^+$ (red) and $[C_{2,1}C_1im]^+$ (black) cations.

practically identical. It is therefore apparent that not all properties are equally affected by alkyl chain branching. Unfortunately, no conclusive results can be deduced from Fig. 7 as, although $[C_3C_1im]^+$ qualitatively appears to be more flexible, practically the energy differences between the two cations are minor, approaching the method's accuracy limits.

The interpretation of Fig. 7 is further complicated by the qualitative differences in the geometry and thus the conformational space. The $[C_3C_1im]^+$ cation shows a preference for the two degenerate structures where the side chain is oriented normal to the ring plane. For the isopropyl side chain in $[C_{2,1}C_1im]^+$, three structures with a C–C bond in the side chain normal to the ring plane are observed. First, in the global minimum structure at 240°, the two methyl groups of the side chain are on either side of the plane, and the hydrogen atom at the tertiary carbon is in the ring plane on the C^2 side. In the two structures with a C–N–C–N dihedral angle of 25° and 100°, the hydrogen atom is on the $C^{4/5}$ side of the ring, and one of the two methyl groups of the isopropyl side chain is oriented normal to the plane.

Only the $[C_3C_1im]^+$ cation exhibits a minimum for the flat structure with a C–N–C–C dihedral angle of 0° (360°). This structure is higher in energy than the global minimum, however the energy difference as well as the barrier separating the conformers is insignificant.

The comparison between the aforementioned cations and $[C_2C_1C_1im]^+$ is very interesting, as this cation is also a structural isomer of the other two and might be expected to share some of their behaviour. We can clearly observe that $[C_2C_1C_1im]^+$ shares more in common, in regards of its flexibility with $[C_3C_1C_1im]^+$ than its structural isomers. This happens because the flexibility of the cation is mostly dominated by the methylation of C^2 position of imidazolium ring, which makes the otherwise allowed flat orientation no longer accessible. However, the physical properties of the occurring salts are affected by a variety of different parameters, apart from the flexibility. Comparing the three structural isomers we see that there are properties, such as thermal transitions, which significantly differ among all three of them (for Br^- salts we have high melting points for $[C_2C_1C_1im]^+$ and $[C_{2,1}C_1im]^+$ and a non-crystallising liquid for $[C_3C_1im]^+$), while other properties like density and viscosity seem to not be affected by the linear or branched arrangement of carbons on the side chain, but are affected by the methylation of C^2 position.

It is noteworthy that the energy profiles for the fluorine and hydroxyl functionalised ions are almost identical (Fig. 8). For the non-methylated analogues (Fig. 8a) the energy difference between the two cations is very small and within the method's accuracy and therefore it can be considered as negligible. The energy profile of $[C_3C_1im]^+$ appears similar but more flattened (less energy difference between the minima and maxima), which could be translated to increased flexibility, and hence the lower viscosity of the $[C_3C_1im][NTf_2]$ IL compared to these functionalised analogues, as transitions between different orientations are feasible energetically.[27] Since the preferred arrangements of CNCC dihedral angles are identical for the

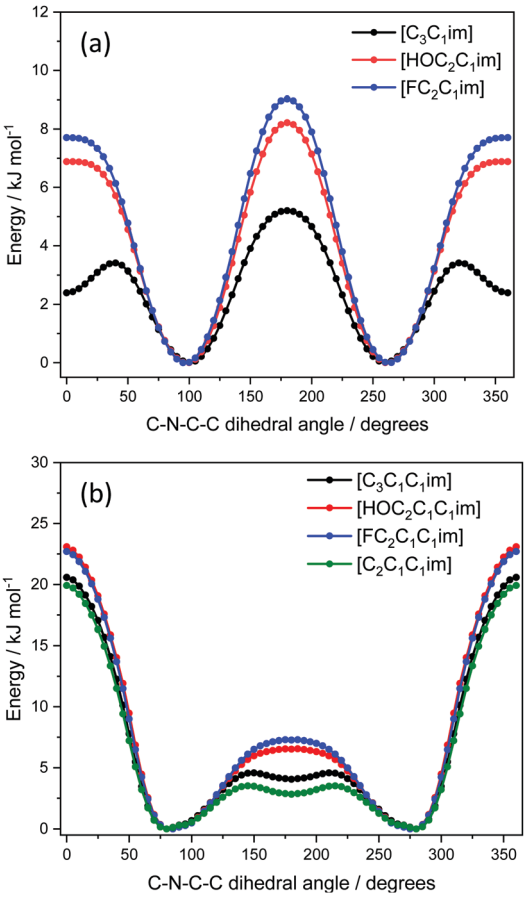

Fig. 8 *Ab initio* energy calculation of C–N–C–C dihedral angle for (a) $[C_3C_1im]^+$ (black) and $[HOC_2C_1im]^+$ (red) and $[FC_2C_1im]^+$ cations and (b) $[C_3C_1C_1im]^+$ (black) and $[HOC_2C_1C_1im]^+$ (red), $[FC_2C_1C_1im]^+$ (blue) and $[C_2C_1C_1im]^+$ (green) cations.

functionalised analogues, and taking into account the experimental measurements, we can conclude that the additional hydrogen bonding site of the hydroxyl group in the alkyl tail is the most likely cause of the viscosity increase of $[HOC_2C_1im][NTf_2]$ compared to $[FC_2C_1im][NTf_2]$ (especially since the end-tail interactions are not taken into account in our calculations). Thus, due to their similar mass and conformational space, $[HOC_2C_1im][NTf_2]$ and $[FC_2C_1im][NTf_2]$ are excellent targeted modifications to investigate hydrogen bonding. We expanded our calculations, in order to theoretically investigate the methylated analogues (although the $[HOC_2C_1im]^+$ and $[FC_2C_1C_1im]^+$ cations were not experimentally studied). All these observations are verified in the case of methylated analogues (Fig. 8b), as we can easily see that the energy profiles are identical, regardless of the functionalisation of the side chain.

As we can see from Fig. 9a, the energy profiles for the triple bond-functionalised non-methylated ions are similar to each other, but are significantly different compared to those of the ions with a saturated side chain. The 0° flat orientation has turned to a global minimum, which indicates the ions' preference of this orientation. The preference for the flat conformer can be rationalised with the efficient delocalisation

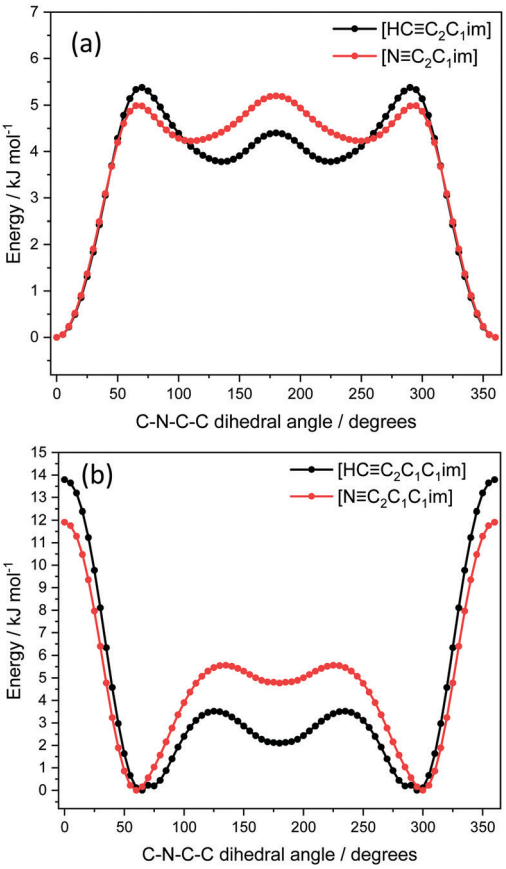

Fig. 9 *Ab initio* energy calculation of C–N–C–C dihedral angle for (a) [HC$\equiv$C$_2$C$_1$im] (black) and [N$\equiv$C$_2$C$_1$im] (red) and (b) [HC$\equiv$C$_2$C$_1$C$_1$im] (black) and [N$\equiv$C$_2$C$_1$C$_1$im] (red) cations.

over the side chain, see Fig. 10, extending the π-system of the ring. Nevertheless, the profile is significantly different for the methylated analogues (Fig. 9b), similar to the other studied methylated structures. The energy increase of the 0° flat orientation in the case of the 2-methylated analogues is the result of steric hindrance due to the presence of the methyl group.[62] The side chain functionalisation seems to affect the minimum energy orientation angles (for methylated triple-bond cations shifted to 60/300° compared to 100/260° for the F- and HO-functionalisations, for methylated triple bond cations shifted to 55/300° compared to 70/270° for the F- and HO-functionalisations – see Fig. 9b), but the overall profile remains in each case qualitatively similar.

Crystallography studies

In the sections above we have presented experimental and theoretical studies, indicating that there is a diverse set of interactions in our studied set of ILs, which significantly affects structuring and properties. Single crystal X-ray crystallography can be used as a valuable tool to verify the effects of different interactions in the structure of the salts and also cross-check the accuracy of the *ab initio* calculations and our understanding of the underlying interactions. Hydrogen bonding will be a main aspect of our analysis, since it is yet widely accepted that

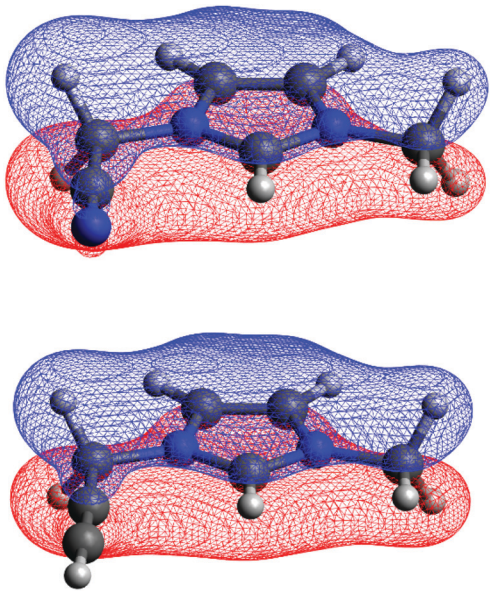

Fig. 10 Molecular orbitals showing efficient electronic delocalisation in flat orientation for [N$\equiv$C$_2$C$_1$im]$^+$ (HOMO−13, top) and [HC$\equiv$C$_2$C$_1$im]$^+$ (HOMO−12, bottom).

hydrogen bonds in ILs are quite diverse in terms of strength and characteristics and they are crucial for the occurring properties.[61]

Analysis of hydrogen bonding

When analysing hydrogen bonding within the structures, the criteria of Jeffrey and Steiner were used.[66,67] These criteria place a strong emphasis on the D–H$\cdots$A distances and angles: shorter distances indicate stronger hydrogen bonds, as does the increasing linearity of the DHA angle. A summary of the solid-state hydrogen bonding interactions in our compounds is shown in Table 4.

In all the compounds we studied, no hydrogen bonds were consistent with the strict criteria for a "strong" hydrogen bond (D$\cdots$A $<$ 2.5 Å; DHA $>$ 170°). Considering that strong hydrogen bonds typically involve molecules like water, protic acids or strong Lewis bases, this is unsurprising. However, it is worth noting that the Jeffrey and Steiner criteria are based on donor and acceptor atoms both being second row elements (*i.e.* C, N, O, F). Heavier elements such as Br are significantly larger than 2p elements and this must be accounted for when classifying the strength of hydrogen bonding.[68,69] A pertinent example is the OH$\cdots$Br bond in [HOC$_2$C$_1$im]Br involving the alcohol group on the cation and the bromide anion (Table 4). This bond is almost linear but the O–Br distance is ∼0.73 Å longer than the strict cut-off for a strong hydrogen bond. Considering the difference in ionic radii of 0.67 Å between Br$^-$ (1.82 Å) and the corresponding 2p element (F$^-$: 1.15 Å for a 2-coordinate ion),[70] then this bond is worth considering as a strong hydrogen bond even though it does not meet the strict Jeffrey and Steiner criteria.

In imidazolium salts, for example [C$_2$C$_1$im]Br, the strongest hydrogen bond donor is normally the C^2–H position (between the two nitrogen atoms) with C$^{4/5}$–H being markedly weaker

Table 4 Summary of hydrogen bonding interactions in the structures described in this paper

	H2–X		H4/5–X		CN–H4/5		Other	
	Distance	Angle	Distance	Angle	Distance	Angle	Distance	Angle
$[C_2C_1im]Br$[a]	3.575	150.32	3.820	164.07				
$[C_2C_1C_1im]Br$			3.652	168.63				
			3.620	162.06				
$[N{\equiv}C_2C_1im]Br$	3.516	154.59	3.626	155.97	3.230	121.75		
$[HC{\equiv}C_2C_1C_1im]Br$							3.638[d]	176.14
$[HC{\equiv}C_2C_1im]Br$	3.516	152.00					3.748[d]	165.30
$[N{\equiv}C_2C_1C_1im]Br$			3.615	148.98	3.326	137.68		
$[N{\equiv}C_2C_1C_1im][NTf_2]$			3.377[b]	158.97[b]				
			3.337[c]	141.13[c]				
			3.449[c]	164.18[c]				
$[N{\equiv}C_2C_1im]Cl$	3.360	154.40	3.459	161.70	3.204	127.32		
$[N{\equiv}C_2C_1C_1im]Cl$			3.550	149.90	3.248	124.71		
			3.473	137.03				
$[HOC_2C_1im]Br$	3.628	153.26	3.730	165.47			3.170[e]	148.99[e]
							3.233[f]	175.15[f]

[a] Data from ref. 73. [b] Molecule 1 in the asymmetric unit and X=O of NTf_2^-. [c] Molecule 2 in the asymmetric unit where X=O of NTf_2^-. [d] Interaction between alkyne CH and Br. [e] HO–H4/5 where OH is acceptor. [f] Br–HO where OH is donor.

hydrogen bond donors.[71] Our results (Table 4) are consistent with this trend: compounds which contain both C^2–H and $C^{4/5}$–H protons all show slightly stronger hydrogen bonding through the C^2–H position. However, it is noteworthy that $[HC{\equiv}C_2C_1C_1im]Br$ and $[HC{\equiv}C_2C_1im]Br$ also contain a terminal alkyne substituent on one of the side chains and, in both compounds, there is no hydrogen bonding involving the $C^{4/5}$–H positions of the imidazolium ring. Instead, the terminal alkyne C–H acts as a weak hydrogen bond donor to the bromide anion. Terminal alkynes are known to be weak hydrogen bond donors to π-systems of alkynes, aromatic rings and other Lewis bases.[72] Here it is likely that the flexibility of the methylene group allows the alkyne to rotate and point towards the bromide ion, forming highly linear hydrogen bonds. It is also important to note that $[HC{\equiv}C_2C_1im]Br$, which has both the C^2–H and the alkyne functional group, prioritises the C^2–H position as the strongest hydrogen bond donor: the alkyne CH···Br distance is 0.1 Å longer than in $[HC{\equiv}C_2C_1C_1im]Br$ (where there is no C^2–H position) and markedly less linear. Thus, we can tentatively form a series of hydrogen bond donor group strength: C^2–H > alkyne > $C^{4/5}$–H. This will be strengthened by future crystallographic studies.

Although nitrile and terminal alkyne groups are isoelectronic, they act as different components of a hydrogen bond and this affects the structure which is generated. For example, $[N{\equiv}C_2C_1im]Br$, and $[HC{\equiv}C_2C_1im]Br$, are structurally identical apart from CN *vs.* CCH, but the unit cell parameters are markedly different. It can also be seen from the bond length data that the nitrile group is a weaker hydrogen bond acceptor than halides. For structures that have both halide and nitrile (*e.g.* $[N{\equiv}C_2C_1im]Br$), the nitrile generally has shorter CH···N distances than corresponding CH···X distances. However, once the size difference between N (second row element) and Cl^- or Br^- (third/fourth row respectively) is accounted for, the halides form stronger hydrogen bonds. The CH···A angles are also consistent with this; the hydrogen bonds involving nitrile are all much more bent than those involving halides.

We also studied the effect of changing the halide anion. In $[N{\equiv}C_2C_1im]Br$ and $[N{\equiv}C_2C_1im]Cl$, the structures are isomorphous and isostructural (aside from a slight contraction in the cell parameters to reflect the smaller size of Cl^- compared to Br^-). Even the hydrogen bond strength appears to be identical, when a ~0.15 Å difference in ionic radius between Br^- and Cl^- is considered. However, the related structures with C^2-methylated imidazolium cations shows a marked difference when the halide is changed from bromide ($[N{\equiv}C_2C_1C_1im]Br$) to chloride ($[N{\equiv}C_2C_1C_1im]Cl$). The crystal system changes from primitive monoclinic to C-centred monoclinic, and one additional hydrogen bond is noted through the imidazolium $C^{4/5}$–H protons. This reflects the strength of hydrogen bonding through the C^2–H position; the ions pack in a way which accommodates the formation of this hydrogen bond. Conversely, the weaker hydrogen bonds formed through $C^{4/5}$–H are not strong enough to influence packing and in this case it is likely that ion size effects dominate the packing, rather than the formation of any particular hydrogen bond. For the imidazolium salts with methylated C^2 position, we also examined the interactions where the anion is positioned directly above the imidazolium ring. No correlations between the strength of these interactions and other physical properties of the salts were noted, but a more detailed crystallographic analysis is presented in the ESI.†

In compound $[N{\equiv}C_2C_1C_1im][NTf_2]$, the combination of the imidazolium cation with a weakly coordinating anion was expected to yield an ionic liquid at room temperature. Instead, a crystalline solid formed. Although the $[NTf_2]^-$ anion is commonly thought of as a weakly coordinating anion, it does have several hydrogen bond acceptor groups and we have previously observed that $[NTf_2]^-$ can form multiple hydrogen bonds with olefinic CH protons in the Cy3 molecular dye, leading to surprisingly large structural deformations in a supposedly planar cation.[74] In $[N{\equiv}C_2C_1C_1im][NTf_2]$, multiple hydrogen bonds are formed between the $C^{4/5}$–H protons and oxygen atoms of the $[NTf_2]^-$ anion, leading to two

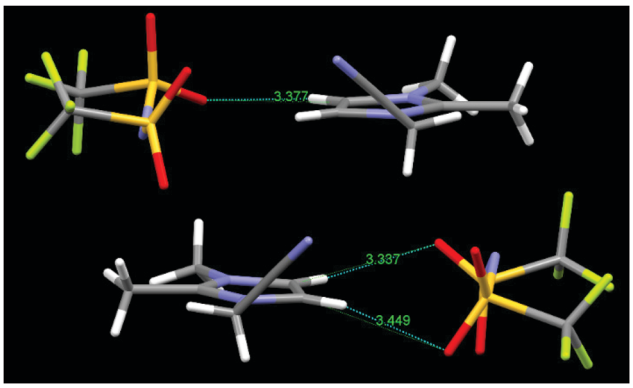

Fig. 11 Diagram showing the hydrogen bonding between nitrile-substituted imidazolium cation and $[NTf_2]^-$ anion in $[N{\equiv}C_2C_1C_1im][NTf_2]$.

symmetry-independent $[NTf_2]^-$ anions in the asymmetric unit (Fig. 11). This regular ordering of $[NTf_2]^-$ anions and imidazolium cations is likely a major reason why $[N{\equiv}C_2C_1C_1im][NTf_2]$ solidified at room temperature.

Preferable orientations

Interestingly, we observe that the crystal structures of some of the synthesised salts (Table 5) do not take the minimum energy orientation, as was predicted by *ab initio* calculations. Fig. 12a shows that halide salts with $[N{\equiv}C_2C_1im]^+$ do have the minimum energy orientation, however this is not the case for $[HC{\equiv}C_2C_1im]^+$ (Fig. 12b), where the crystal structure is approximately on the midpoint of the energy barrier. The most significant deviation is observed for the $[N{\equiv}C_2C_1C_1im]^+$ salts (Fig. 12c), where the halides are around the minimum energy position, but the $[NTf_2]^-$ salt falls on a local maximum. Crystallography indicates that is probably a packing effect, since the anion is large compared to the cation and 'forces' it to a specific structure in order to fit. Because of this deviation in $[N{\equiv}C_2C_1C_1im][NTf_2]$, it would be interesting to optimise the periodic crystal structure at an *ab initio* level of theory. A study of non-covalent interactions would enable further insight into why this situation arises. However, such a study would be far beyond the scope of this work.

Table 5 Three-bond C(2)–N(2)–C(5)–C(6) torsion angles for the structures described in this paper. Note: (a) two symmetry-independent cations in the asymmetric unit

Ionic liquid	CNCC angle
$[N{\equiv}C_2C_1im]Br$	0.000(1)
$[HC{\equiv}C_1C_2C_1im]Br$	−62.1(2)
$[HC{\equiv}C_2C_1im]Br$	−40.6(5)
$[N{\equiv}C_2C_1C_1im]Br$	−77.1(9)
$[N{\equiv}C_2C_1C_1im][NTf_2]$	137.6(5)
	130.7(6)
$[N{\equiv}C_2C_1im]Cl$	0.000(0)
$[N{\equiv}C_2C_1C_1im]Cl$	−76.2(2)
$[HOC_2C_1im]Br$	85.2(10)

Fig. S40c (see ESI†) shows that $[N{\equiv}C_2C_1C_1im]Br$ and Cl^- salts could form structures in which cations interact with each other *via* the nitrile side chain. These dipolar interactions between cyano groups have been observed in a few other organic crystal structures of neutral molecules,[75,76] however here we observe that they are favoured even for charged species, which are naturally repelled. However, this is not the case for the $[NTf_2]^-$ salt, for which we do not see any cation–cation interactions from the X-ray crystallography, probably a result of packing effects due to the size of the anion. Further information about these dipolar interactions between the nitrile functionalised cations are provided in the ESI.†

$[HOC_2C_1im]Br$ shows an exact match between the theoretically calculated energy minimum and the CNCC angle measured with X-ray crystallography. As it can be seen in Fig. S48 (see ESI†) the additional hydrogen bonding between the terminal OH group of the alkyl chain and the Br^- anion affects the position of Br^- ion relative to the imidazolium ring, but does affect the minimum energy orientation compared to the non-functionalised analogues.

MD simulations

Complementary MD simulations were performed on $[C_2C_1im][NTf_2]$ and $[C_2C_1C_1im][NTf_2]$ to facilitate the interpretation of our experimental results. These two model systems were chosen as they represent the simplest cases in terms of functionalisation (one for non-methylated and one for methylated C^2 position of the imidazolium ring) and yet give a dramatic change in physical properties. Interactions involving

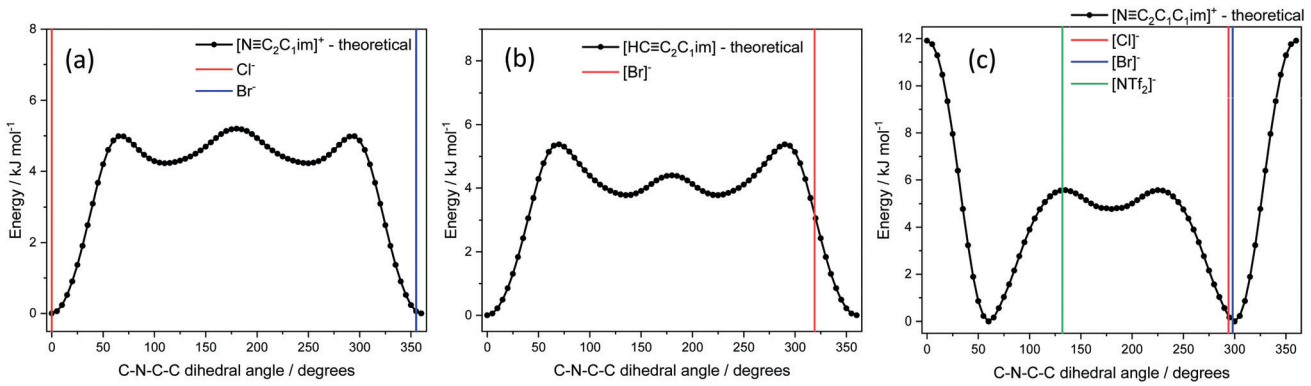

Fig. 12 Comparison between *ab initio* energy calculations and C–N–C–C dihedral angles received by X-ray crystallography studies.

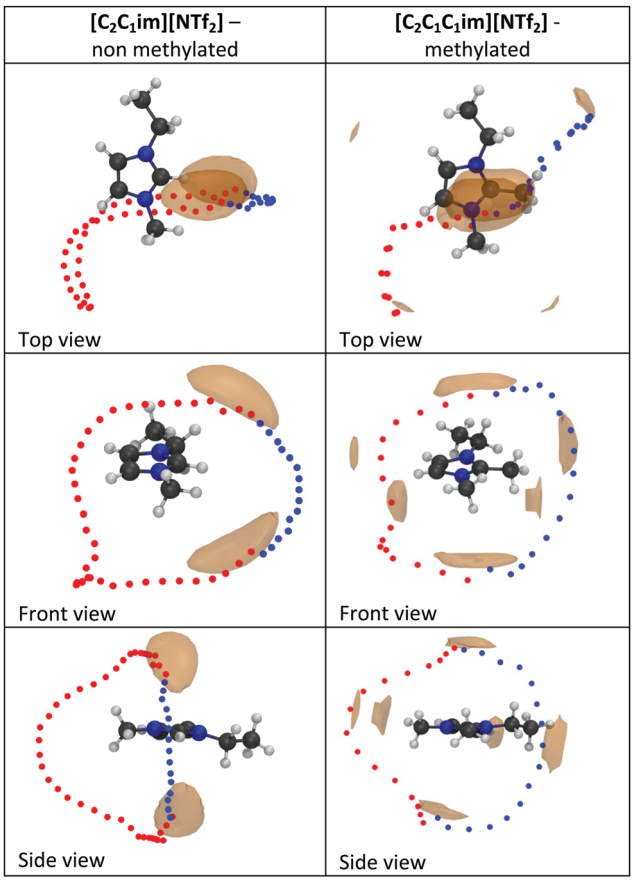

Fig. 13 MD results for $[C_2C_1im][NTf_2]$ and $[C_2C_1C_1im][NTf_2]$. The red and blue beads show the minimum energy paths obtained with a nudged elastic band optimizer. The transparent orange regions are isosurfaces at 75% probability of the highest peak in the spatial distribution function. Top view: view normal to plane, front view: view along N–N bond, methyl group in the foreground tilted down, side view: view along the C^2–H bond. Beads represent the centre of mass for the NTf_2 anion. Attached in the ESI,† are short videos of these pictures.

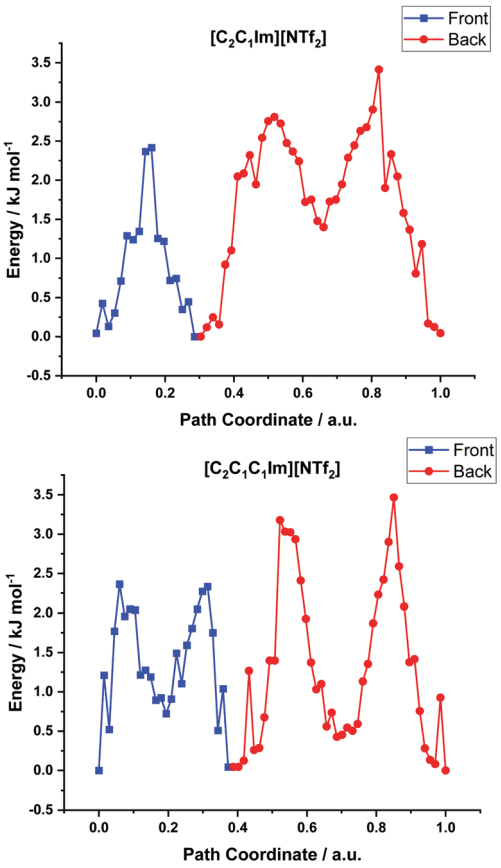

Fig. 14 Energy to path coordinate graphs for the studied ILs.

functional groups in the side chains will naturally influence the results; however, this would be beyond the scope of this work.

The MD simulations reveal (Fig. 13) that methylation of the C^2 position significantly changes the preferred location of the $[NTf_2]^-$ anion. For both cations, the highest values in the spatial distribution functions are found on either side of the imidazolium ring plane. For $[C_2C_1im][NTf_2]$, the preferred positions are shifted towards the space surrounding the acidic C^2–H, whereas for $[C_2C_1C_1im][NTf_2]$ they are centred over the imidazolium ring. This is in line with the observations made by Zhang *et al.* on $[C_4C_1im][PF_6]$ and $[C_4C_1C_1im][PF_6]$.[77]

Further insight is provided using the potential of mean force, eqn (1).

$$w(\xi) = -k_B T \ln g(\xi) \quad (1)$$

Here, w is the potential of mean force, ξ is the path coordinate, k_B is the Boltzmann constant, T is the thermodynamic temperature, g is the value of the spatial distribution function. Thus, the beads in Fig. 13 correspond to the minimum (free) energy path connecting the arrangements of anions around the cation which are statistically lowest in energy. The energy along this path is shown in Fig. 14. It is evident that the barriers involved in the path on the $C^{4/5}$ side of the ring are comparable for the two cations. In contrast, the potential of mean force is very different for the path on the C^2 side of the ring. First, the barriers are slightly larger for $[C_2C_1C_1im][NTf_2]$ compared to $[C_2C_1im][NTf_2]$. Second, the minimum energy path connecting the two preferred locations is considerably longer and more corrugated in the case of $[C_2C_1C_1im][NTf_2]$, and the anion has to pass through an additional minimum. Hence, in agreement with the literature, our simulations show that there is a mostly entropic cost in terms of anion mobility when the C^2 position is methylated.[78,79]

Conclusions

In this work we investigated the structure–property relationship of a series of dialkylimidazolium ILs, with different functionalisations of the side chain. All the salts were made with appropriate heteroatoms, in order for the molecular weight to not deviate more than 5% from our reference cation, which is $[C_3C_1im]^+$. We performed a thorough study of bulk properties for those ILs, which effectively revealed that changing the terminal functional group can affect each studied property

differently, sometimes in unexpected ways. Characteristic examples of these behaviours are the cases of terminal F-group substitution, which affects the decomposition pathway for the halide salts, but not for $[NTf_2]^-$ salts or any other property. In an analogous way, changing from linear to branched chain (cases of $[C_3C_1im]^+$ and $[C_{2,1}C_1im]^+$ as well as their C^2-methylated analogues) does not seem to have a significant effect in any of the studied transport properties, but it does affect the thermal properties. In order to analyse and interpret these observations, we performed *ab initio* theoretical calculations of the minimum energy orientations for our studied structures.

Since some of the studied salts were solid around room temperature, we performed a crystallographic analysis to gain insight regarding the effect of the alkyl chain functionalisation on the hydrogen bonding strength and even compare the effect of different anions on the obtained structures. Of great interest to our study is the case of the $[N\equiv C_2C_1C_1im]^+$ salts, and especially $[N\equiv C_2C_1C_1im][NTf_2]$, which surprisingly to us is a high-melting point solid. Crystallography and *ab initio* calculations helped us to elucidate part of this behaviour, however further studies could be performed in order to gain a clearer understanding of this behaviour.

The final point that needed to be explained was the large differences that in most measurements appear between the methylated and non-methylated analogues of each set (consistently higher viscosities, higher decomposition temperatures, higher melting points and lower diffusion rates for the methylated analogues). To address this issue, we performed MD simulations in the simplest IL cases, namely $[C_2C_1im][NTf_2]$ and $[C_2C_1C_1im][NTf_2]$. These simulations were in agreement with previous works on similar systems and revealed that C^2 methylation significantly changes the preferred position of the anion and also reduces the mobility of the anion (entropic cost). Of course, it is expected that the functionalisation of the side chain will further affect the simulation results and this could be a future continuation of this work.

All the results presented in this work agree with our initial hypothesis. ILs are complex systems and their physical properties are affected by a wide array of different parameters. In almost every one of the studied properties there was one IL that behaved unexpectedly and usually these were different ILs in each case. This certainly indicates that our current understanding of IL chemistry is not sufficient to predict the properties of new ionic liquids (even for simple molecular structures such as the alkylimidazolium cation) and that such fundamental studies are more relevant than ever. Our findings indicate that researchers need to be extremely cautious when they use data on one family of ILs to extrapolate and predict the behaviour of another family of ILs. Interpolation among ILs of the same family is a safer route, but this still requires a sufficiently thorough dataset and the use of a properly trained statistical model.[18] Understanding simple molecular structures is the first step that needs to be taken, followed by the investigation of more complex systems of industrial interest.

Author contributions

Conceptualization S. K., T. W.; supervision T. W.; investigation S. K., F. P., D. R., D. P.; methodology S. K., F. P., D. R., D. P.; writing – original draft preparation S. K., F. P., D. P.; writing – review & editing, S. K., F. P., D. R., D. P., C. W. M. K., T. W.

Conflicts of interest

There are no conflicts to declare.

Acknowledgements

The authors thank Kateryna Goloviznina and Agílio A. H. Pádua for providing the force fields. Authors thank Svenja Pohl for helping with the TGA/MS measurements. Authors also thank Peter Haycock and Corey Fulop for PFGSE NMR measurements, Lisa Haigh for the mass spectra and Andrew White for X-ray crystallography measurements. Computational resources provided by the Imperial College Research Computing Service are gratefully acknowledged. DOI: 10.14469/hpc/2232. F. P. acknowledges funding from the President's PhD scholarship.

Notes and references

1 T. Welton, *Biophys. Rev.*, 2018, **10**, 691–706.
2 G.-T. Wei, Z. Yang and C.-J. Chen, *Anal. Chim. Acta*, 2003, **488**, 183–192.
3 M. Galiński, A. Lewandowski and I. Stępniak, *Electrochim. Acta*, 2006, **51**, 5567–5580.
4 M. Armand, F. Endres, D. R. MacFarlane, H. Ohno and B. Scrosati, *Mater. Sustainable Energy*, 2011, 129–137.
5 S. Koutsoukos, T. Tsiaka, A. Tzani, P. Zoumpoulakis and A. Detsi, *J. Cleaner Prod.*, 2019, **241**, 118384.
6 M. Freemantle, *Chem. Eng. News*, 1998, **76**, 32–37.
7 G. M. Kontogeorgis, R. Dohrn, I. G. Economou, J.-C. de Hemptinne, A. Ten Kate, S. Kuitunen, M. Mooijer, L. F. Žilnik and V. Vesovic, *Ind. Eng. Chem. Res.*, 2021, **60**, 4987–5013.
8 A. Noda, K. Hayamizu and M. Watanabe, *J. Phys. Chem. B*, 2001, **105**, 4603–4610.
9 M. Ue, M. Takeda, A. Toriumi, A. Kominato, R. Hagiwara and Y. Ito, *J. Electrochem. Soc.*, 2003, **150**, A499.
10 J. Jacquemin, P. Husson, A. A. Padua and V. Majer, *Green Chem.*, 2006, **8**, 172–180.
11 D. R. MacFarlane, J. Golding, S. Forsyth, M. Forsyth and G. B. Deacon, *Chem. Commun.*, 2001, 1430–1431.
12 F. Philippi, D. Rauber, J. Zapp, C. Präsang, D. Scheschkewitz and R. Hempelmann, *ChemPhysChem*, 2019, **20**, 443–455.
13 H. Li, M. Ibrahim, I. Agberemi and M. N. Kobrak, *J. Chem. Phys.*, 2008, **129**, 124507.
14 M. Salanne, C. Simon, P. Turq and P. A. Madden, *J. Phys. Chem. B*, 2007, **111**, 4678–4684.
15 Y. Qiao, Y. Ma, Y. Huo, P. Ma and S. Xia, *J. Chem. Thermodyn.*, 2010, **42**, 852–855.

16 J. Jacquemin, R. Ge, P. Nancarrow, D. W. Rooney, M. F. Costa Gomes, A. A. Pádua and C. Hardacre, *J. Chem. Eng. Data*, 2008, **53**, 716–726.
17 K. Paduszynski and U. Domanska, *J. Chem. Inf. Model.*, 2014, **54**, 1311–1324.
18 S. Koutsoukos, F. Philippi, F. Malaret and T. Welton, *Chem. Sci.*, 2021, **12**, 6820–6843.
19 F. Philippi and T. Welton, *Phys. Chem. Chem. Phys.*, 2021, **23**, 6993–7021.
20 P. Bonhote, A.-P. Dias, N. Papageorgiou, K. Kalyanasundaram and M. Grätzel, *Inorg. Chem.*, 1996, **35**, 1168–1178.
21 M. Sorai and K. Saito, *Chem. Rec.*, 2003, **3**, 29–39.
22 I. Krossing, J. M. Slattery, C. Daguenet, P. J. Dyson, A. Oleinikova and H. Weingärtner, *J. Am. Chem. Soc.*, 2006, **128**, 13427–13434.
23 T. Endo, S. Hoshino, Y. Shimizu, K. Fujii and K. Nishikawa, *J. Phys. Chem. B*, 2016, **120**, 10336–10349.
24 M. Van Oort and M. White, *Thermochim. Acta*, 1985, **86**, 1–6.
25 D. C. Belchior, T. E. Sintra, P. J. Carvalho, M. R. Soromenho, J. M. Esperança, S. P. Ventura, R. D. Rogers, J. A. Coutinho and M. G. Freire, *J. Chem. Phys.*, 2018, **148**, 193842.
26 D. Rauber, F. Philippi, J. Zapp, G. Kickelbick, H. Natter and R. Hempelmann, *RSC Adv.*, 2018, **8**, 41639–41650.
27 F. Philippi, D. Pugh, D. Rauber, T. Welton and P. A. Hunt, *Chem. Sci.*, 2020, **11**, 6405–6422.
28 CrysAlisPro, Yarnton, Oxfordshire, England, 2014.
29 O. V. Dolomanov, L. J. Bourhis, R. J. Gildea, J. A. Howard and H. Puschmann, *J. Appl. Crystallogr.*, 2009, **42**, 339–341.
30 C. F. Macrae, I. Sovago, S. J. Cottrell, P. T. Galek, P. McCabe, E. Pidcock, M. Platings, G. P. Shields, J. S. Stevens and M. Towler, *J. Appl. Crystallogr.*, 2020, **53**, 226–235.
31 M. J. Frisch, G. W. Trucks, H. B. Schlegel, G. E. Scuseria, M. A. Robb, J. R. Cheeseman, G. Scalmani, V. Barone, B. Mennucci, G. A. Petersson, H. Nakatsuji, M. Caricato, X. Li, H. P. Hratchian, A. F. Izmaylov, J. Bloino, G. Zheng, J. L. Sonnenberg, M. Hada, M. Ehara, K. Toyota, R. Fukuda, J. Hasegawa, M. Ishida, T. Nakajima, Y. Honda, O. Kitao, H. Nakai, T. Vreven, J. J. A. Montgomery, J. E. Peralta, F. Ogliaro, M. Bearpark, J. J. Heyd, E. Brothers, K. N. Kudin, V. N. Staroverov, T. Keith, R. Kobayashi, J. Normand, K. Raghavachari, A. Rendell, J. C. Burant, S. S. Iyengar, J. Tomasi, M. Cossi, N. Rega, J. M. Millam, M. Klene, J. E. Knox, J. B. Cross, V. Bakken, C. Adamo, J. Jaramillo, R. Gomperts, R. E. Stratmann, O. Yazyev, A. J. Austin, R. Cammi, C. Pomelli, J. W. Ochterski, R. L. Martin, K. Morokuma, V. G. Zakrzewski, G. A. Voth, P. Salvador, J. J. Dannenberg, S. Dapprich, A. D. Daniels, O. Farkas, J. B. Foresman, J. V. Ortiz, J. Cioslowski and D. J. Fox, *Gaussian, Inc.*, Gaussian, Inc., Wallingford CT, 2013.
32 S. Ehrlich, J. Moellmann, W. Reckien, T. Bredow and S. Grimme, *ChemPhysChem*, 2011, **12**, 3414–3420.
33 S. Grimme, S. Ehrlich and L. Goerigk, *J. Comput. Chem.*, 2011, **32**, 1456–1465.
34 D. C. Prieve and W. B. Russel, *J. Colloid Interface Sci.*, 1988, **125**, 1–13.
35 K. Goloviznina, Z. Gong, M. F. Costa Gomes and A. A. Pádua, *J. Chem. Theory Comput.*, 2021, **17**, 1606–1617.
36 H. Sun, *J. Phys. Chem. B*, 1998, **102**, 7338.
37 J. H. Jonkman, J. Wijsbeek, S. H. B. D. Boer, R. A. de Zeeuw, L. Van Bork and N. Orie, *J. Pharm. Pharmacol.*, 1975, **27**, 849–854.
38 J. N. Canongia Lopes, J. Deschamps and A. A. Pádua, *J. Phys. Chem. B*, 2004, **108**, 2038–2047.
39 J. N. C. Lopes and A. A. Pádua, *Theor. Chem. Acc.*, 2012, **131**, 1–11.
40 J. N. Canongia Lopes and A. A. Pádua, *J. Phys. Chem. B*, 2006, **110**, 19586–19592.
41 C. Y. Son, J. G. McDaniel, Q. Cui and A. Yethiraj, *J. Phys. Chem. Lett.*, 2019, **10**, 7523–7530.
42 J. E. Basconi and M. R. Shirts, *J. Chem. Theory Comput.*, 2013, **9**, 2887–2899.
43 W. Shinoda, M. Shiga and M. Mikami, *Phys. Rev. B: Condens. Matter Mater. Phys.*, 2004, **69**, 134103.
44 J. Li, A. H. Ngan and P. Gumbsch, *Acta Mater.*, 2003, **51**, 5711–5742.
45 K. Goloviznina, Z. Gong and A. A. Padua, *Wiley Interdiscip. Rev.: Comput. Mol. Sci.*, 2021, e1572.
46 G. Lamoureux and B. Roux, *J. Chem. Phys.*, 2003, **119**, 3025–3039.
47 E. Heid, A. Szabadi and C. Schröder, *Phys. Chem. Chem. Phys.*, 2018, **20**, 10992–10996.
48 K. Goloviznina, J. N. Canongia Lopes, M. Costa Gomes and A. A. Pádua, *J. Chem. Theory Comput.*, 2019, **15**, 5858–5871.
49 A. A. Pádua, *J. Chem. Phys.*, 2017, **146**, 204501.
50 C. Maton, N. De Vos and C. V. Stevens, *Chem. Soc. Rev.*, 2013, **42**, 5963–5977.
51 J. P. Paraknowitsch and A. Thomas, *Macromol. Chem. Phys.*, 2012, **213**, 1132–1145.
52 K. R. Lovelock, J. P. Armstrong, P. Licence and R. G. Jones, *Phys. Chem. Chem. Phys.*, 2014, **16**, 1339–1353.
53 J. P. Paraknowitsch, A. Thomas and M. Antonietti, *J. Mater. Chem.*, 2010, **20**, 6746–6758.
54 G. Konstantopoulos, S. Soulis, D. Dragatogiannis and C. Charitidis, *Materials*, 2020, **13**, 2749.
55 J. S. Lee, X. Wang, H. Luo, G. A. Baker and S. Dai, *J. Am. Chem. Soc.*, 2009, **131**, 4596–4597.
56 S. Zhang, K. Dokko and M. Watanabe, *Mater. Horiz.*, 2015, **2**, 168–197.
57 Y. Zhang, L. Xue, F. Khabaz, R. Doerfler, E. L. Quitevis, R. Khare and E. J. Maginn, *J. Phys. Chem. B*, 2015, **119**, 14934–14944.
58 L. Xue, E. Gurung, G. Tamas, Y. P. Koh, M. Shadeck, S. L. Simon, M. Maroncelli and E. L. Quitevis, *J. Chem. Eng. Data*, 2016, **61**, 1078–1091.
59 J. N. Canongia Lopes, M. F. Costa Gomes and A. A. Pádua, *J. Phys. Chem. B*, 2006, **110**, 16816–16818.
60 S. Tsuzuki, H. Matsumoto, W. Shinoda and M. Mikami, *Phys. Chem. Chem. Phys.*, 2011, **13**, 5987–5993.
61 P. A. Hunt, C. R. Ashworth and R. P. Matthews, *Chem. Soc. Rev.*, 2015, **44**, 1257–1288.
62 P. A. Hunt, *J. Phys. Chem. B*, 2007, **111**, 4844–4853.

63 K. R. Harris and M. Kanakubo, *Phys. Chem. Chem. Phys.*, 2015, **17**, 23977–23993.
64 S. Tsuzuki, *ChemPhysChem*, 2012, **13**, 1664–1670.
65 C. Rey-Castro, A. Tormo and L. F. Vega, *Fluid Phase Equilib.*, 2007, **256**, 62–69.
66 G. Jeffrey, *An Introduction to Hydrogen Bonding*, Oxford University Press, New York, 1997.
67 T. Steiner, *Angew. Chem., Int. Ed.*, 2002, **41**, 48–76.
68 W. Levason, D. Pugh and G. Reid, *New J. Chem.*, 2017, **41**, 1677–1686.
69 M. J. Champion, W. Levason, D. Pugh and G. Reid, *New J. Chem.*, 2016, **40**, 7181–7189.
70 R. D. Shannon, *Acta Crystallogr., Sect. A: Cryst. Phys., Diffr., Theor. Gen. Crystallogr.*, 1976, **32**, 751–767.
71 P. N. Bartlett, C. Y. Cummings, W. Levason, D. Pugh and G. Reid, *Chemistry*, 2014, **20**, 5019.
72 T. Steiner, *Adv. Mol. Struct. Res.*, 1998, **4**, 43–78.
73 A. Elaiwi, P. B. Hitchcock, K. R. Seddon, N. Srinivasan, Y.-M. Tan, T. Welton and J. A. Zora, *J. Chem. Soc., Dalton Trans.*, 1995, 3467–3472.
74 R. Clark, M. A. Nawawi, A. Dobre, D. Pugh, Q. Liu, A. P. Ivanov, A. J. White, J. B. Edel, M. K. Kuimova and A. J. McIntosh, *Chem. Sci.*, 2020, **11**, 6121–6133.
75 P. A. Wood, S. J. Borwick, D. J. Watkin, W. S. Motherwell and F. H. Allen, *Acta Crystallogr., Sect. D: Struct. Biol.*, 2008, **64**, 393–396.
76 S. Lee, A. B. Mallik and D. C. Fredrickson, *Cryst. Growth Des.*, 2004, **4**, 279–290.
77 Y. Zhang and E. J. Maginn, *Phys. Chem. Chem. Phys.*, 2012, **14**, 12157–12164.
78 S. Zahn, G. Bruns, J. Thar and B. Kirchner, *Phys. Chem. Chem. Phys.*, 2008, **10**, 6921–6924.
79 A. S. Rodrigues, C. F. Lima, J. A. Coutinho and L. M. Santos, *Phys. Chem. Chem. Phys.*, 2017, **19**, 5326–5332.